Supplementary Information

Engineering charge transfer in a two-dimensional S-scheme heterojunction photocatalyst *via* built-in electric field for selective biomass valorization

Taolian Guo[a,#,], Rong Dang[a,#], Anyu Zheng[b], Shaodan Wang[c], Xiongwei Dong[a], Zhongduo Xiong[d], Zibo Chen[e], Zifu Hu[a], Wu Chen[a,]*, Chao Wang[b,]**

[a]National Local Joint Engineering Laboratory for Advanced Textile Processing and Clean Production, Wuhan Textile University, Wuhan 430200, China

[b]School of Chemistry and Chemical Engineering, Yangzhou University, Yangzhou 225002, China

[c]College of Chemistry, Central China Normal University, Wuhan 430079, China

[d]Analytical and Testing Center, Wuhan Textile University, Wuhan 430200, China

[e]Sanya Science and Education Innovation Park, Wuhan University of Technology, Sanya 572000, China

[#]These authors contributed equally to this work.

*To whom correspondence should be addressed. E-mail addresses: tlguo@wtu.edu.cn (T. Guo); wuchen@wtu.edu.cn (W. Chen); wangchao@yzu.edu.cn (C. Wang)

Experimental section

Materials. All solvents and reagents were purchased from commercial sources and used without further purification. N,N-dimethylformamide (DMF, AR), ethanol (AR), acetonitrile (HPLC), isopropanol were purchased from Sinopharm Chemical Reagent Co., Ltd. 2-aminoterephthalic acid, titanium tetraisopropanolate, potassium iodide (KI), ammonium formate (HPLC, ≥99.0%) and 5-hydroxymethylfuran (HMF) were purchased from Aladdin. Zinc chloride ($ZnCl_3$), indium chloride ($InCl_3$), thioacetamide (TAA), sodium iodate ($NaIO_3$), 1,4-benzoquine(PBQ), 5-hydroxymethyl-2-furancarboxylic acid (HMFCA), 2,5-furandicarbaldehyde (DFF) and 5-formyl-2-furoic Acid (FFCA) were purchased from Macklin. 1,4-Diaza[2.2.2] Bicyclooctane were purchased from Tokyo Chemical Industry (TCI)**.**

Synthesis of bulk NMT (NH_2-MIL-125 (Ti)). Typically,[1] In a typical synthesis, $H_2BDC\text{-}NH_2$ (0.28 g) and tetra-n-butyl titanate ($Ti(OC_4H_9)_4$, 0.3 mL) were dissolved in a mixed solvent containing DMF (9 mL) and methanol (1 mL), followed by being transferred into a 20 mL Teflon-lined stainless steel autoclave and heated at 150 °C for 72 h. Subsequently, the product was collected by centrifugation and washed thoroughly with DMF and ethanol, and dried at 60 °C under vacuum overnight.

Characterizations. The crystalline structure of as-synthesized samples was characterized by an X-ray diffractometer (XRD, Bruker D8 Advance, Germany) using Cu Kα radiation (40 KV, 40 mA). The Ultraviolet-visible diffuse reflectance spectra (UV-vis DRS) were obtained by Shimadzu UV-2600. Fourier transform Infrared (FT-IR) spectrum using the KBr pellet was measured on a Brucker Tensor 27 in the range of 4000-500 cm^{-1}. The morphology and microstructure of samples were observed by field-emission scanning electron microscope (SEM, Crossbeam 350, Zeiss) and transmission electron microscope (TEM, FEI Tecnai G2 F30). The high-resolution TEM image of NMT nanosheets was taken under low-voltage mode with a low electron dose (FEI Tecnai G^2 F20, 60 kV, 34.2 e^- $Å^{-2}$ s^{-1}). X-ray photoelectron spectroscopy (XPS) spectra were recorded using Escalab 250Xi instrument (Thermo Scientific) equipped with an Al Kα microfocused X-ray source. The porosity structure and specific surface area were studied by nitrogen adsorption-desorption measurements using an Autosorb IQ

Chemisorption/Physisorption Analyzer (ASAP 2460-4MP). Electron paramagnetic resonance (EPR) signals were recorded on an EMXplus-6/1 spectrometer (Bruker A300, Germany) with addition of 5,5-dimethyl-1-pyrroline N-oxide (DMPO) to trap $\bullet O_2^-$. The steady-state photoluminescence (PL) spectra and time-resolved photoluminescence (TRPL) decay plots were detected by the spectrophotometer with an excitation wavelength of 375 nm. Besides, the photoelectrochemical properties of samples were measured using an electrochemical workstation (CHI660E). The ITO substrates coated with samples were employed as the working electrodes with a working electrode area of 1 cm^2. The Pt and Ag/AgCl electrodes were used as counter and reference electrodes, and 0.5 M Na_2SO_4 was used as the electrolyte, respectively. Photocurrent experiments were performed under Xe lamp. Mott Schottky plots were measured at alternating current frequencies.

Theoretical calculations. Density function theory (DFT) calculations were performed by using the CP2K-2022.1 package. Perdew-Burke-7 (PBE) of functional was used to describe the system. Unrestricted Kohn-Sham DFT has been used as the electronic structure method in the framework of the Gaussian and plane waves (GPW) way. The Goedecker-Teter-Hutter (GTH) pseudopotentials and Double-ζ molecularly optimized basis sets (DZVP-MOLOPT-GTH) have been used for all elements. The Brillouin zone was sampled with gamma points for surface calculation. A plane-wave energy cutoff of 400 Ry (1Ry = 13.606 eV) has been employed. The geometries were optimized using the Broyden-Fletcher-Goldfarb-Shanno (BFGS) algorithm. The convergence threshold of density matrix during self-consistent field (SCF) method was $1*10^{-5}$ Hartree, and convergence criterion for the forces was set to $4.5*10^{-4}$ Bohr/Hartree.[2] A vacuum layer of 15 Å was constructed to eliminate interactions between periodic structures of surface models. The van der Waals (vdW) interaction was amended by the DFT-D3 method of Grimme.

Supplementary Figures and Tables

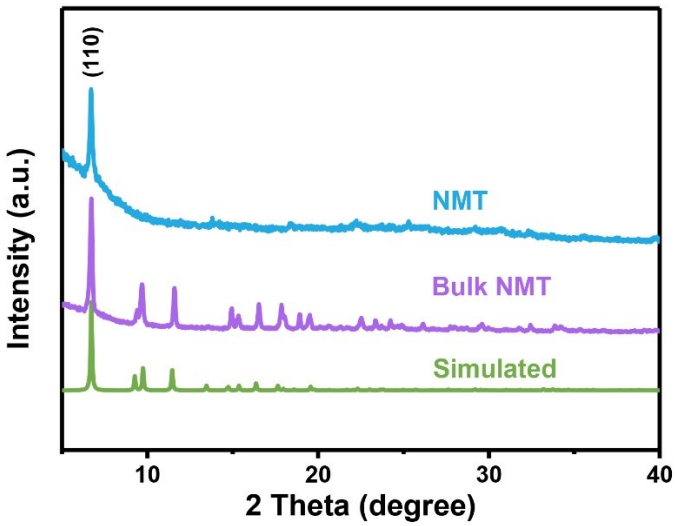

Fig. S1 XRD patterns of NMT, bulk NMT, and simulated NMT.

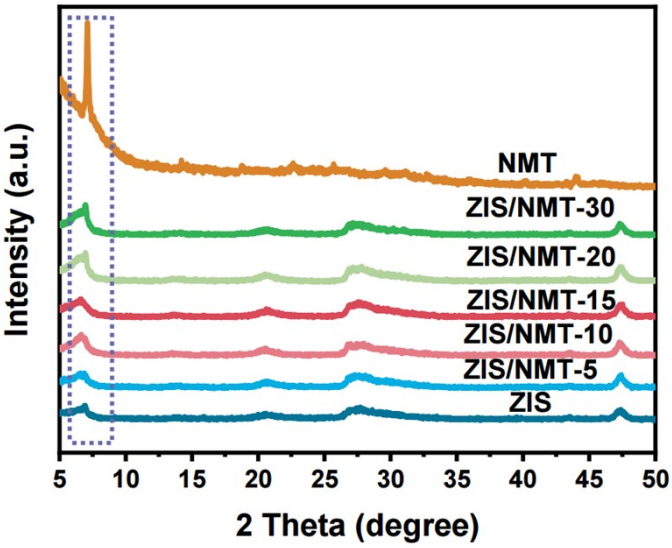

Fig. S2 XRD patterns of NMT, ZIS and ZIS/NMT-X.

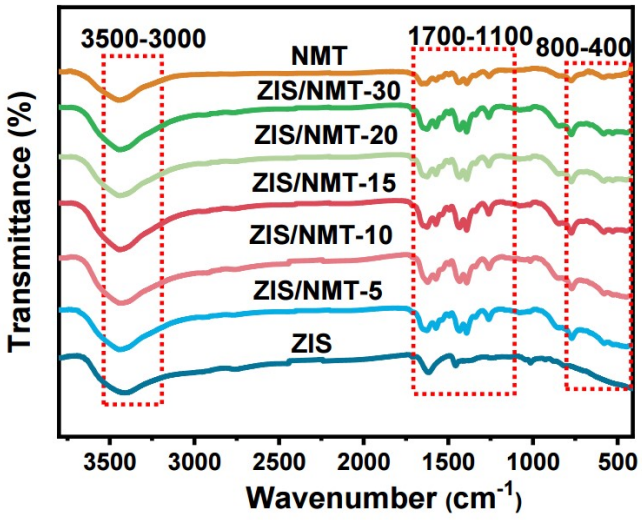

Fig. S3 FT-IR spectra of NMT, ZIS and ZIS/NMT-X.

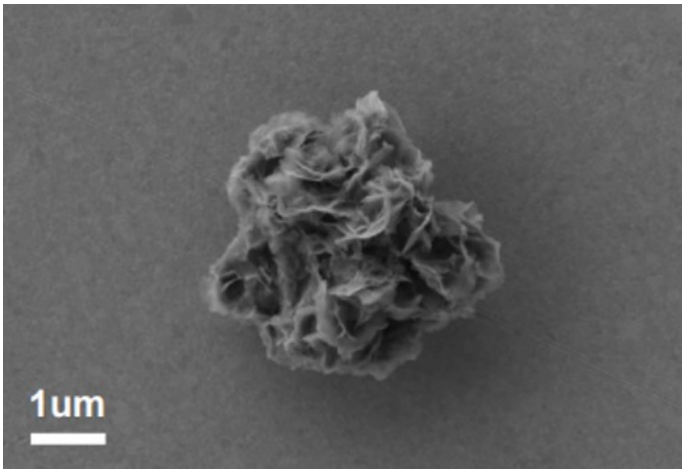

Fig. S4 SEM image of NMT.

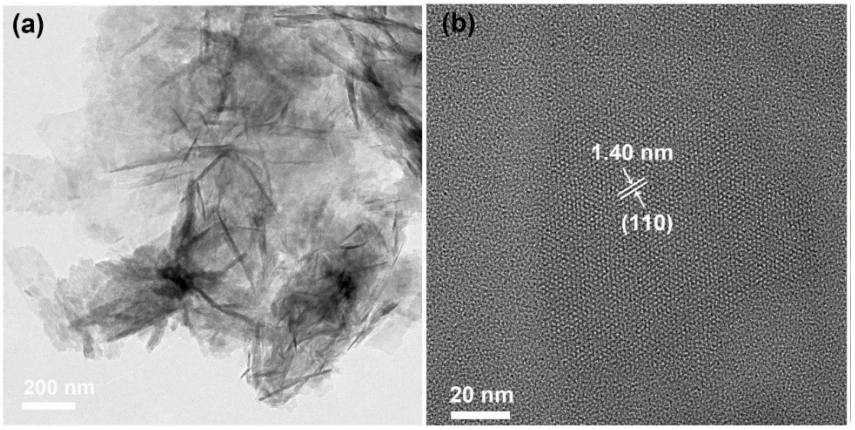

Fig. S5 (a) TEM and (b) HRTEM images of NMT.

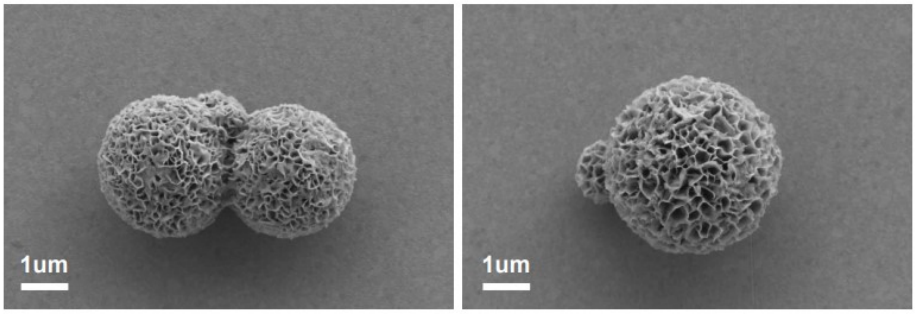

Fig. S6 SEM images of bare ZIS.

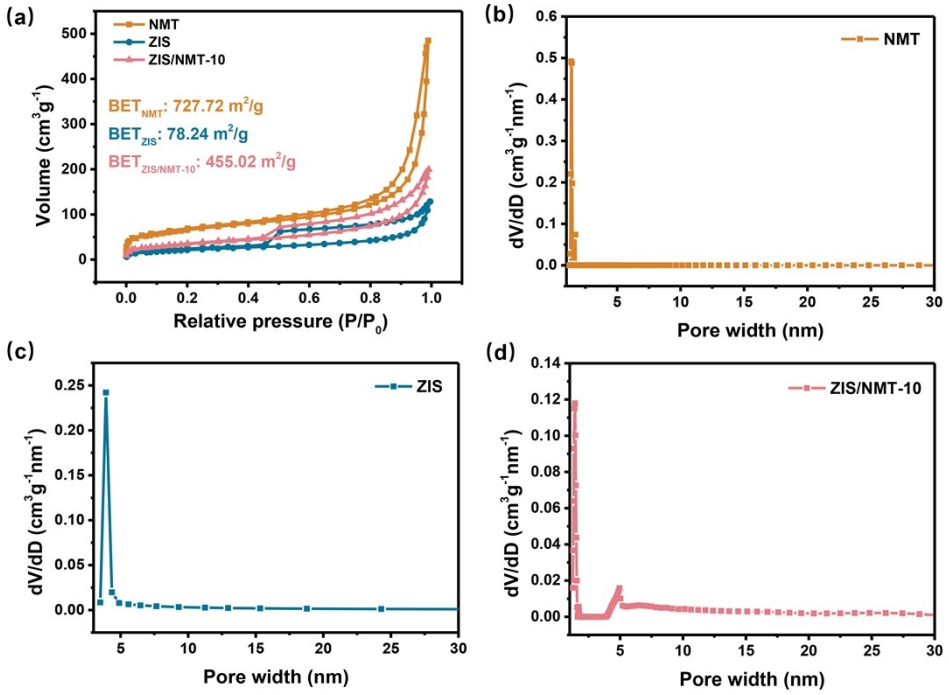

Fig. S7 (a) N_2 absorption-desorption isotherms of NMT, ZIS and ZIS/NMT-10. (b-d) Related pore size distribution profiles.

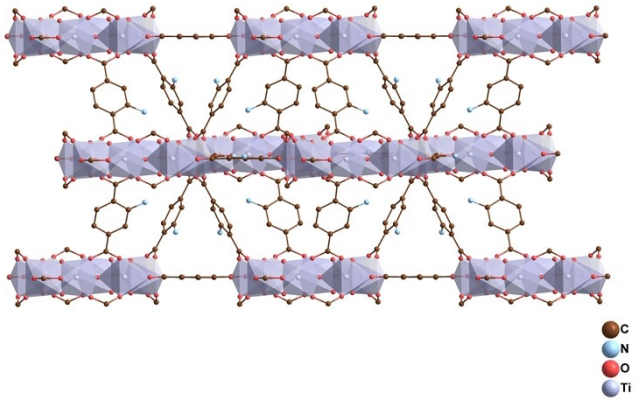

Fig. S8 Structure of NMT.[1]

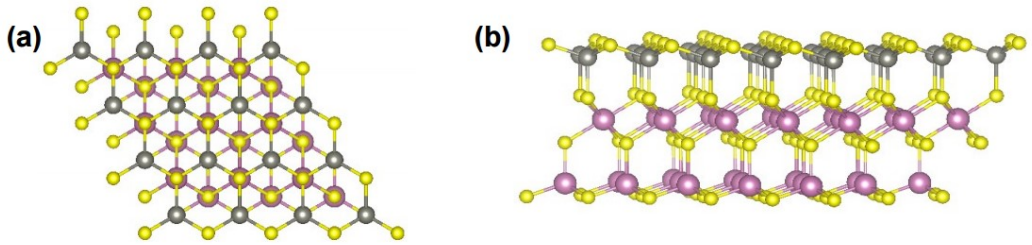

Fig. S9 (a) Top view and (b) side view of the optimized structure of ZIS.

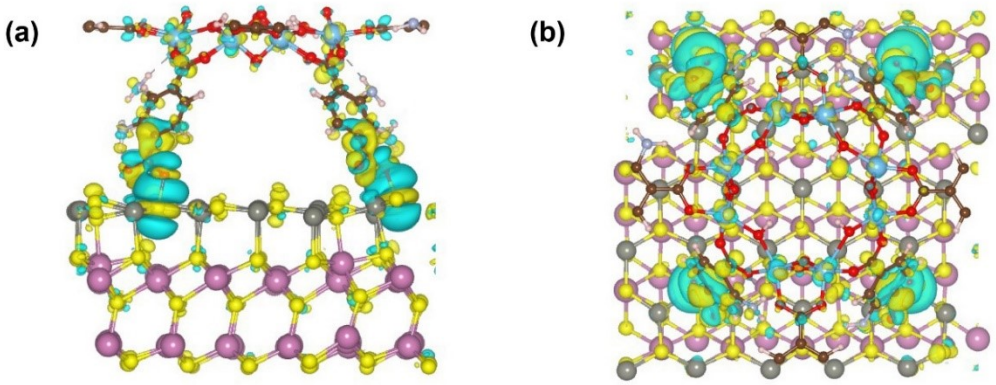

Fig. S10 (a) Side view and (b) top view of the charge density difference of ZIS/NMT heterojunction. The charge accumulation and charge depletion are shown in the yellow and cyan regions, respectively.

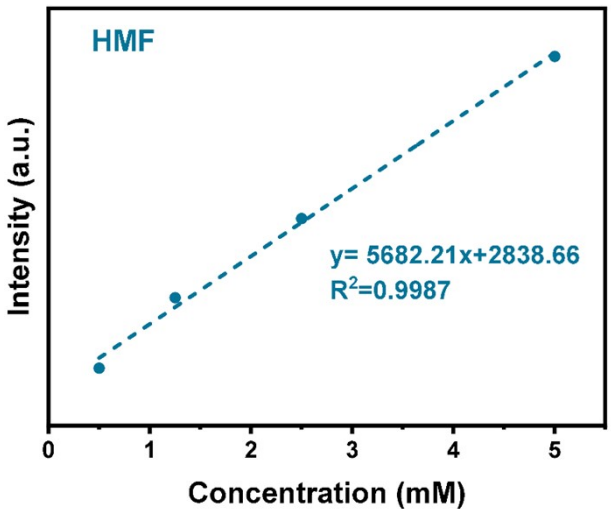

Fig. S11 Linear regression proving formula for HMF.

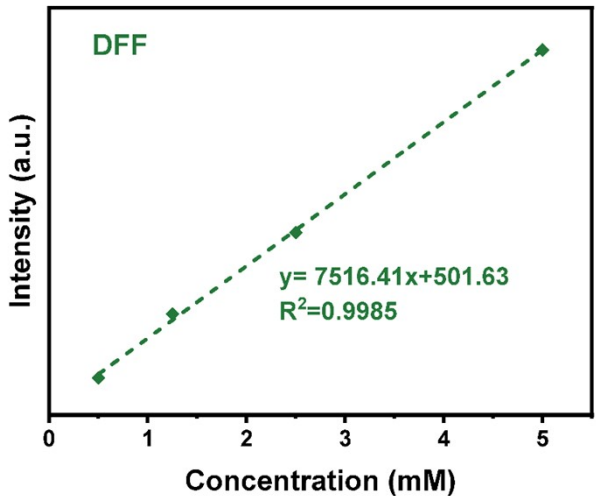

Fig. S12 Linear regression proving formula for DFF.

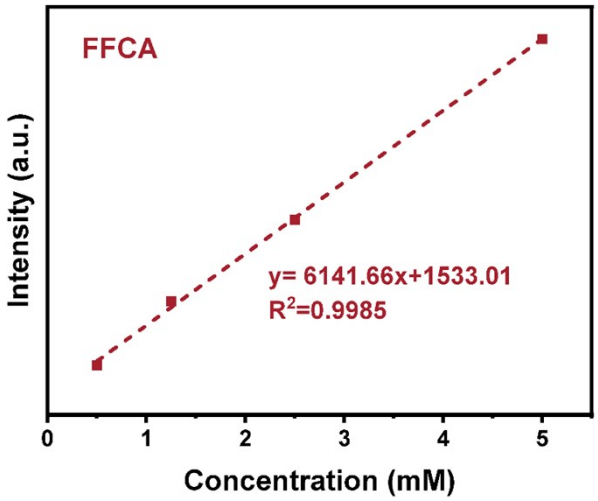

Fig. S13 Linear regression proving formula for FFCA.

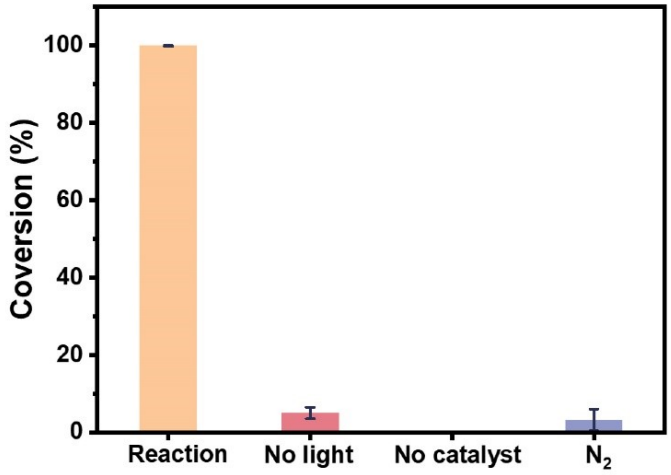

Fig. S14 Blank control experiments for HMF oxidation over NMT/ZIS-10.

Table S1. Results of HMF photocatalysis under different conditions.

Entry	Catalyst	HMF Con. (%)	DFF Sel. (%)	HMFCA Sel. (%)	FFCA Sel. (%)
1	ZIS	75.7	68.2	-	-
2	NMT	26.1	-	99	-
3	ZIS/NMT-5	>99	13.8	-	86.2
4	ZIS/NMT-10	>99	7.5	-	92.5
5	ZIS/NMT-15	98.2	60.4	-	39.6
6	ZIS/NMT-20	94.5	64.5	-	35.5
7	ZIS/NMT-30	87.1	82.7	-	17.3
8	ZIS+NMT	87.1	86.3	-	13.7

Reaction conditions: HMF (5 mM, 5 mL, aqueous), photocatalyst (40.0 mg), room temperature, reaction time (14 h), light source (white LED).

Table S2. Comparison of photocatalytic HMF conversion results with related studies.

Entry	Catalyst	Light source	HMF Con. (%)	DFF Sel. (%)	HMFCA Sel. (%)	FFCA Sel. (%)	Ref.
1	ZIS/NMT-10	40 W LED	>99	7.5	-	92.5	Ours
2	g-C_3N_4/$NaNbO_3$	300 W Xe	35.2	-	-	87.4	[3]
3	ZnS/ZIS	500 W Xe	100	70.9	-	-	[4]
4	MNs/CIS	500 W Xe	78.5	76.8	-	-	[5]
5	$Cd_{1.5}In_2S_{4.5}$	500 W Xe	68.8	62.7	-	-	[6]
6	Au/TiO_2	Xe lamp	99	-	95	-	[7]
7	TiO_2@UiO-67	300 W Xe	94	70	-	-	[8]

Table S3. The results of HMF photocatalysis in different conditions.

Entry	Condition	HMF Con (%)
1	Reaction	>99
2	No catalyst	Not detected
3	No light (in darkness)	5.0
4	N_2	3.2

Reaction conditions: HMF (5 mM, 5 mL), photocatalyst (40.0 mg), room temperature, reaction time (14 h).

Table S4. The results of HMF photocatalysis in different scavengers.

Entry	Condition	HMF Con (%)
1	None	>99
2	DABCO	89.8
3	KI	61.5
4	IPA	>99
5	$NaIO_3$	7.1
6	PBQ	Not detected

Reaction conditions: HMF (5 mM, 5 ml), photocatalyst (40.0 mg), scavengers (5 mM), room temperature, reaction time (14 h).

References

[1] C. Wang, Q. Xie, T. Guo, M. Fang, W. Mao, Y. Zhang, H. Wang, X. Ma, Y. Wu, S. Li and J. Han, *Nano Lett.*, 2023, **23**, 10930-10938.

[2] T. Lu and F. Chen, *J. Comput. Chem.*, 2012, **33**, 580-592.

[3] Y. Zhu, Y. Zhang, L. Cheng, M. Ismael, Z. Feng and Y. Wu, *Adv. Powder Technol.*, 2020, **31**, 1148-1159.

[4] Y. Zhang, M. Zhang, Z. Yu, R. Liu, Y. Li, J. Xiong, Y. Qiao, R. Zhang and X. Lu, *Appl. Catal.*, *B*, 2024, **350**, 123914.

[5] M. Zhang, Y. Zhang, L. Ye, Z.Yu, R. Liu, Y. Qiao, L. Sun, J. Cui and X. Lu, *Appl. Catal.*, *B*, 2023, **330**, 122635.

[6] M. Zhang, Z. Yu, J. Xiong, R. Zhang, X. Liu and X. Lu, *Appl. Catal.*, *B*, 2022, **300**, 120738.

[7] B. Zhou, J. Song, Z. Zhang, Z. Jiang, P. Zhang and B. Han, *Green Chem.*, 2017, **19**, 1075-1081.

[8] Y. Zhou, J. Liu and J. Long, *J. Solid State Chem.*, 2021, **303**, 122510.